"**Eulerian-Lagrangian Model for the Prediction of Cavitation Erosion**"

Casey Bradt

2.29 Spring 2022 Final Project

Massachusetts Institute of Technology

Introduction

With both environmental benefits of decreased emissions, as well as a cost benefit realized by consumers, developing engines with increased efficiency is a strong incentive for heavy duty diesel engine manufacturers to remain competitive. Two of the main avenues of pursuit in this regard are reducing the frictional losses in the power cylinder system, and increasing the combustion pressure. However, these two goals are not without obstacles, and often stand in conflict with each other. As future designs push for higher combustion pressures, the concomitant issue of coolant cavitation in wet liner engines is likely to increase in salience. Cavitation in the coolant can cause tremendous damage to wet liners, and is often caused by vibrations in the liner driven by piston slap and other piston secondary motion characteristics. With an increase in combustion pressure, the piston secondary motion will also intensify which is expected to exacerbate cavitation damage to the liner. Thus, coolant cavitation is a barrier to higher efficiency engines.

In order to mitigate this coolant cavitation, designers can alter the characteristics of the piston geometry, water jacket geometry, coolant chemical composition, liner material, and various other design variables. However, this is generally done based on engineering judgement and intuition paired with experiment. A widely available model which can quickly and accurately predict cavitation characteristics and optimize design variables to avoid such cavitation is lacking. Additionally, design solutions which effectively mitigate cavitation damage

often come at the expense of altering piston characteristics in a way that increases fictional losses. The ultimate goal of this research is to establish the modeling capability to accurately and quickly simulate cavitation damage driven by piston dynamics, and to develop an optimization framework which can serve to find an optimal design for preventing cavitation damage without significantly increasing frictional losses. To do so, however, requires simulations of multi-physics phenomena and systems level integration of these analyses to form a design methodology. This involves simulating the piston dynamics, structural dynamics of the liner vibration, macro-level fluid flow of in the water jacket, bubble dynamics and cloud cavitation behavior, and material fatigue and damage. The work done for this project will focus on the numerical simulations of one of these physical phenomena, namely the cloud cavitation. We will restrict our focus here to two-phase flow dynamics of a spherical cloud structure with spherical bubbles near a wall with periodically fluctuating pressure.

Governing Physics

The physical behavior of a cavitating flow is governed by two main sets of equations. The first of these is the Navier-Stokes equations given by Equation (1) and Equation (2) below. The Navier-Stokes equations for the mixture phase (average of liquid and vapor phase) are commonly solved for mutli-phase flows and this is the current treatment. Subscript “m” in the following equations denotes the mixture phase.

$$\rho_m \frac{D\mathbf{u}}{Dt} = -\nabla p + \mu_m \nabla^2 \mathbf{u},$$

Equation (1)

$$\frac{1}{\beta}\frac{\partial p}{\partial \tau} + \frac{\partial \rho_m}{\partial t} + \nabla \cdot (\rho_m \mathbf{u}) = 0.$$

Equation (2)

An artificial compressibility term is added to the left-hand side of Equation (2) for the numerical solution. The variable beta represents a numerical parameter which can be changed to control the relative importance of the compressibility term. This compressibility term is then solved for iteratively in pseudo-time (tau) for each physical time step of the variable "t." It is important to mention that we expect the physics of the scenario to be in within the regime of incompressible flow, and that we are using a compressible form of the Navier-Stokes equations strategically for the advent of using a compressible flow solver. Using such an artificial compressibility method is a good choice for bubbly flows because of the change in mixture density as a function of time and space that results from bubbles expanding or shrinking. This change in density as a function of time and space is what happens in compressible flows, although it is caused by different mechanisms, and thus this similarity justifies the use of a compressible flow solver for the multi-phase flow phenomena with which we are interested. The second set of governing equations describe the dynamic behavior of the bubbles themselves, and how they react to and influence the surrounding flow field. This set of equations is given by Equation (3), which describes the trajectory of a bubble, and Equation (4), the Rayleigh-Plesset equation which describes the expansion or shrinkage of a bubble.

$$\frac{d\mathbf{u}_b}{dt} = \left(\frac{\rho_l}{\rho_g}\right)\left[\frac{3}{8R}C_D|\mathbf{u}_s|\mathbf{u}_s + \frac{1}{2}\left(\frac{d\mathbf{u}_{enc}}{dt} - \frac{d\mathbf{u}_b}{dt}\right) - \frac{\nabla p}{\rho_l} + \frac{(\rho_b - \rho_l)}{\rho_l}g + \frac{3C_L}{4\pi}\frac{\sqrt{\nu}}{R}\frac{\mathbf{u}_s \times \boldsymbol{\Omega}}{\sqrt{|\boldsymbol{\Omega}|}} + \frac{3\dot{R}}{2R}\mathbf{u}_s\right],$$

Equation (3)

$$\left(1 - \frac{\dot{R}}{c_m}\right)R\ddot{R} + \frac{3}{2}\left(1 - \frac{\dot{R}}{3c_m}\right)\dot{R} = \frac{\mathbf{u}_s^2}{4} + \frac{1}{\rho_m}\left(1 + \frac{\dot{R}}{c_m} + \frac{R}{c_m}\frac{d}{dt}\right)\left[p_v + p_{g0}\left(\frac{R_0}{R}\right)^{3k} - p_{enc} - \frac{2\gamma}{R} - 4\mu_m\frac{\dot{R}}{R}\right],$$

Equation (4)

The various terms in Equation (3) represent the forces due to drag, mass transfer, pressure gradient field of the liquid fluid, gravity, lift, and the Bjerknes effect of how bubble respond to acoustic waves. The above bubble dynamics equations must be solved on very small timescale and length scale compared to that of the Navier-Stokes equations. This multi-scale nature of this problem presents us with the challenges that computing solutions to these equations is prone to being either extremely computationally intensive on the one hand, or numerically unstable on the other. Wise choice of numerical scheme is then paramount for the successful simulation of this phenomenon.

Domain and Boundary Conditions

In the modeling of this problem, a cube-shaped domain with a side length of 8.5 mm was chosen. The initial radius of the bubble cloud was set to 1.5 mm, which was also the initial stand-off distance (distance from bubble cloud center to the wall). A sinusoidal pressure wave input at the wall (y-

z plane) with a phase of pi was also selected for each case. The amplitude of the wave was changed from case to case, but the phase remained constant throughout all simulations such that pressure at the wall first decreases relative to the ambient baseline pressure and then increases above the ambient later in the period. A constant initial timestep of about 15 ns was used for the solution of the mixture phase fluids, although later studies added the capability of an adaptive timestep to increase the performance of the numerical method. This will be discussed later with the analysis of the solution stability. It is important to note that all dimensional quantities were non-dimensionalized in the solution process according to specified characteristic pressure, length, and velocity (non-zero even when physical free-stream velocity is zero). A picture of the discrete domain grid is shown below in Figure (1).

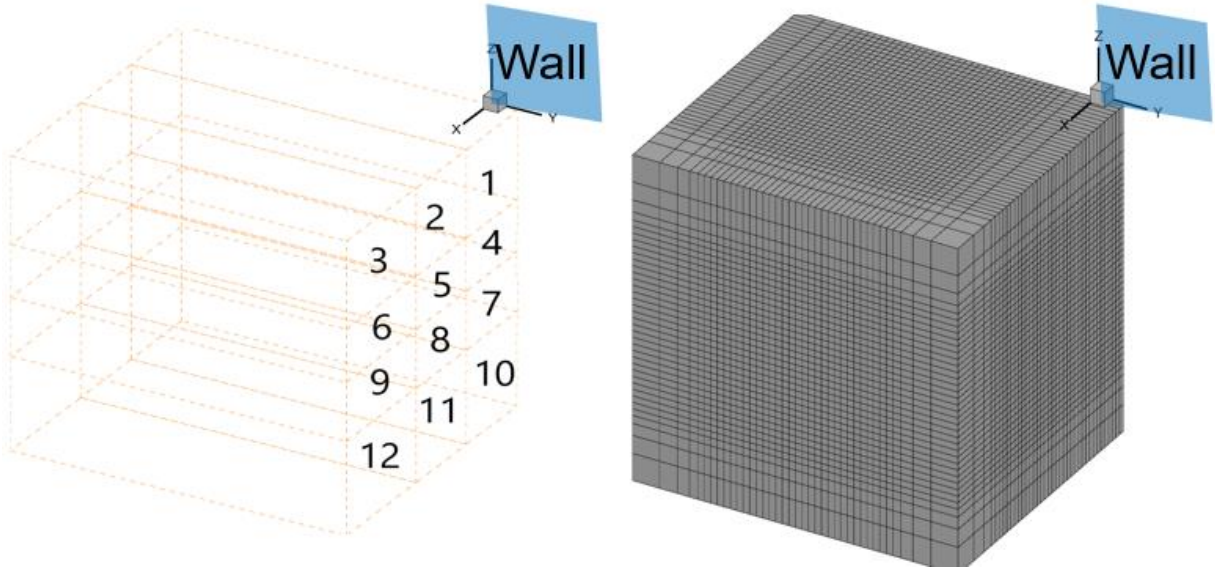

Figure (1)

The left image illustrates the use of a multi-bock method whereby the domain was partitioned into 12 sections, each with their own grid. This was done so that the domain may yield itself well to parallel computing, assigning a processor (or group of processors) to each block. The right image shows the full grid of the domain. A structured grid with uniform spacing of 0.2 mm in the region of the bubble cloud and non-uniform grid spacing along the edges of the domain was used for the early computational

cases. Later cases were run with a different grid. A Dirichlet no-slip boundary condition was applied to the wall, and a free-stream boundary condition was assigned to grid points on the other external “faces” of the cube-shaped grid.

Numerical Solution Techniques

Computation was carried out using a coupling of two packages of a commercial software called 3DynaFS. Numerical solution techniques for multi-phase flows are most commonly done using either Eulerian-Eulerian models, Eulerian-Lagrangian models, or direct numerical simulation. Eulerian-Eulerian models treat the multi-phase flow as two interpenetrating continua, one for the liquid and one for the gas, and local properties for both phases are computed on an Eulerian grid in the “laboratory” (or bulk fluid) frame of reference. Eulerian-Lagrangian models treat gas phase bubbles as singular points in space, tracking the center of each bubble. In this solution method, bulk phase mixture flow properties and the positions of each bubble center are calculated on an Eulerian grid, while the dynamics of each bubble are calculated relative each respective bubble position in a Lagrangian fashion. Direct numerical simulation is not computationally feasible for many practical flows without the use of a peta-scale computer. Additionally, Eulerian-Eulerian models have been known to struggle with high void fraction multi-phase flows. So, an Eulerian-Lagrangian approach is used by the 3DynaFS software here employed. The 3DynaFS-VIS module is a three-dimensional viscus Navier-Stokes solver which is used to compute the mixture phase flow field. This module is coupled with 3DynaFS-DSM which computes the bubble dynamic behavior. The coupling is maintained via computation of the void fraction from the bubble sizes and number in the DSM module and the effect of the void fraction on the local mixture density in the Navier-Stokes equations solved by the VIS module.

For a given case, the user specifies the initial size and position of the bubble cloud, the number of bubbles, and the initial size of the bubbles. Then, the bubbles are initialized at random positions

within these user-specified constraints. Bubbles here were assumed to all be the same size initially with a radius of 50 microns. Additionally, they were assumed to be in equilibrium with the surrounding liquid at time zero. The program conserves the number of bubbles throughout time, modeling bubble collapse as the shrinkage of the bubble to a very small, non-zero size. Finally, the program does not take into account bubble-bubble interaction effects such as bubble breakup or coalescence and does not track the bubble surface. This means that while the bubble center is not allowed to penetrate the wall, the bubble surface may penetrate the wall or other bubbles. The software package does offer the option of preventing bubble surfaces from penetrating other surfaces, but this feature was not enabled for the current study due to a significant increase in computational cost.

The Lagrangian solver (DSM module) typically requires a fine time resolution relative to the Eulerian solver (VIS module). The ramifications and influence of this on the solution are discussed later in a stability analysis. For the cases run in this study, the time resolution of the Lagrangian solver ranged from 50 to 500 times that of the Eulerian solver.

The VIS module is based on finite difference discretization. It uses a 1^{st} order implicit Euler method with Discrete Newton Relaxation in time. The viscous terms of the Navier-Stokes equations are approximated by a second order central differencing scheme and the first and third order terms of the convective fluxes are approximated using Roe's and van Leer's MUSCL methods, respectively. The bubble dynamics equations are ODE's in time and thus are integrated using a fourth order Runge-Kutta method.

Numerical Stability

The simulations run in this study were very prone to numerical instability. Numerical instability was apparent in visualization of the results with the human eye, and examples of a stable versus unstable result is shown in Figure (2).

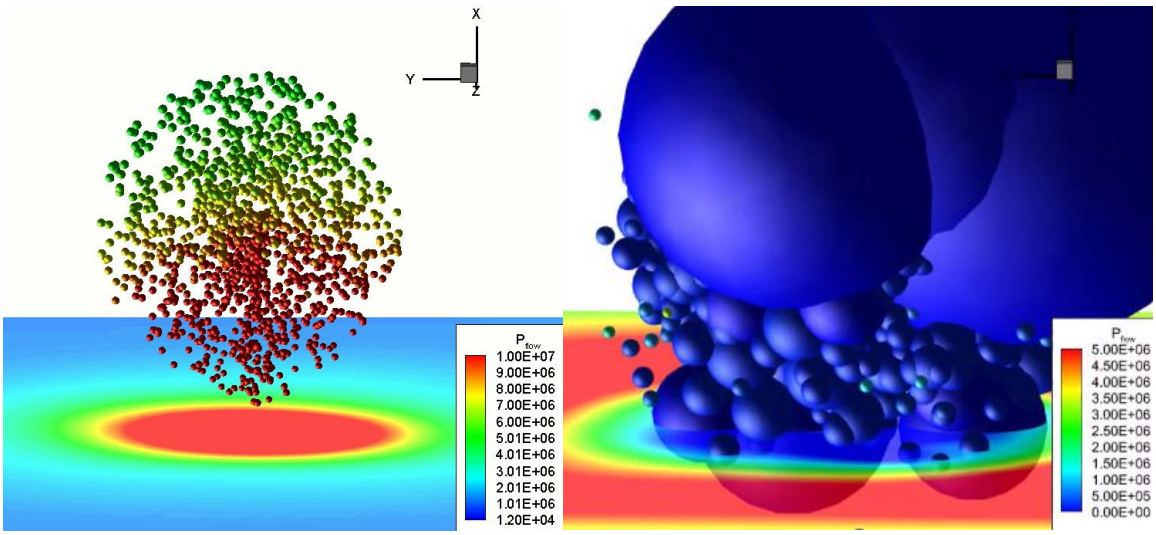

Figure (2) Stable (left) versus unstable (right) results

Because of the complexity of the governing equations and the inaccessibility of the intermediate computational matrices to the program user, matrix and Von Neuman stability analyses are not applicable to our case. Instead, a heuristic stability analysis of sorts was carried out. The first technique investigated for improving numerical stability was the formulation of the void fraction. Traditional computation of the void fraction takes the volume of gas in a computational cell and divides it directly by the total volume of the computational cell. This method can cause large discontinuity between the void fraction calculated in one cell and the void fraction computed in a neighboring cell. From trial and error, this method tends to breed unstable results. So instead, an alternate void fraction formulation was chosen to investigate whether it might enhance the numerical stability of the algorithm. This new formulation represents the vapor fraction contribution of each bubble as a smooth Gaussian function oriented at the center of each bubble and scaled to match the width (diameter) of the bubble. This mathematical representation is given by Equation (5) and Equation (6) below.

$$\alpha_i = \sum_{j=1}^{N_i} \frac{v_{i,j} V_j^b}{\sum_{k}^{N_{\text{cells}}} v_{k,j} V_k^{\text{cell}}}$$

Equation (5)

$$v_{i,j} = \frac{1}{\left(\sqrt{2\pi} R_s\right)^3} e^{-\frac{d_{ij}^2}{2R_s^2}}$$

Equation (6)

Figure (3) shows a visual representation of this void fraction representation.

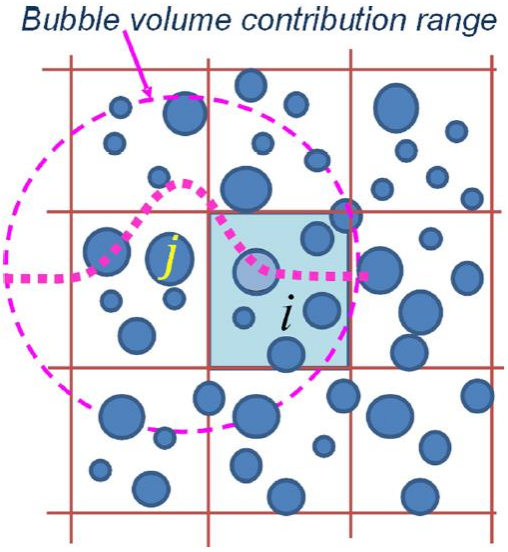

Figure (3)

This method increased the stability of some runs; of the cases run for this study all stable runs used this void fraction formulation.

The second technique investigated for its effect on stability was grid refinement. Figure (4) shows the refined grid used.

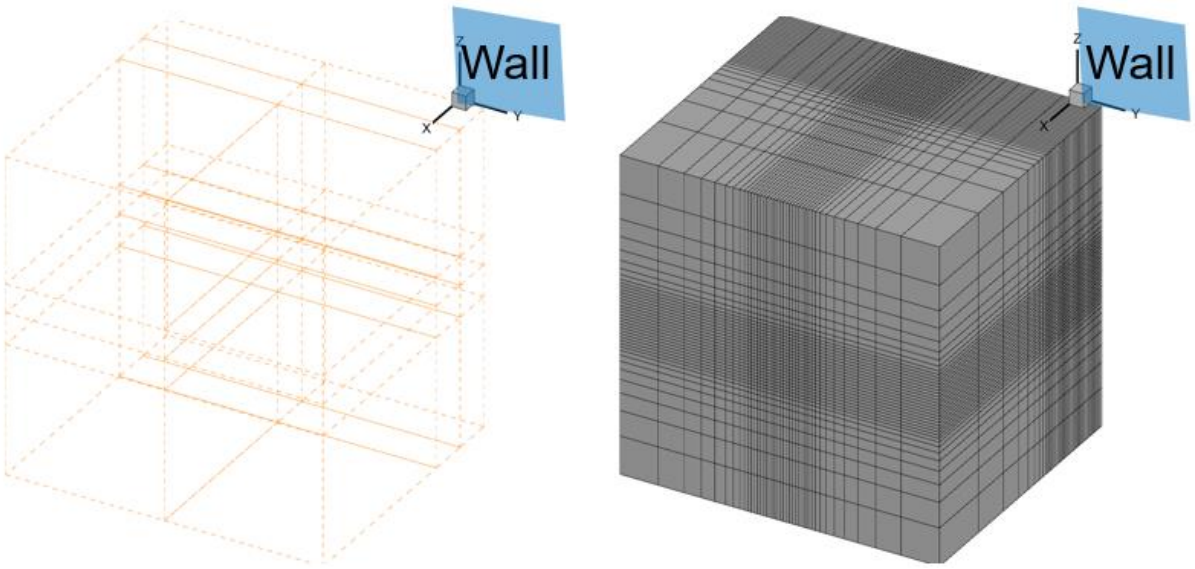

Figure (4)

The grid in Figure (4) still uses a multi-block technique with 12 blocks. However, the spatial resolution of the grid in the region of the bubble cloud is increased from 0.2 mm in the original grid to 0.1 mm in the new grid. Far away from the region of the bubble cloud, the grid size is made more coarse so as to save computational cost in the regions of space where we are not so interested. The time step was not modified for the simulations run on the new grid. Using the speed of sound in water as 1460 m/s, the CFL number for the original grid is 0.0001 and the CFL number for the new grid is 0.0002. Running cases with high pressure inputs are particularly prone to instability, so a case was run on both grids with an ambient pressure of 10 bar, pressure pulse amplitude of 15 bar, and frequency of 5 kHz. With the initial grid, the run became unstable around the time of the maximum input pressure. However, for the new

grid, a stable case was achieved. It is interesting to point out that changing from the an unstable case to a stable one corresponded to an increase of the CFL number. Generally, it is desirable to keep the CFL number low in attempt to achieve numerical stability. In various multi-phase flow simulations reported in literature, it is not uncommon to choose a value such as 0.5, 0.1 or even 0.01 as an upper bound on the CFL number. However, we may also note that having too low a CFL number may result in very high numerical diffusion. This is what we may speculate to be the cause of the result we have observed for an unstable case with a CFL number of 0.0001. Thus, for other unstable cases, it may be advantageous in the future to try re-running them with refined grids which increase the CFL number.

The other parameters investigated for stability effects include the use of an adaptive timestep, the relative timestep size of the Lagragian solver compared to the Eulerian solver, and the artificial compressibility parameter, “beta” (in Equation (2)). An adaptive timestep was computed by taking the average bubble radius at the previous time, dividing by the average velocity of the bubble interface, and further dividing by a user-specified numerical input parameter. This approach proved useful in delaying instability for all of the tested cases, but did not eliminate the instability. Two values were investigated for the ratio of the Lagrangian time step to the Euerian timestep. Firstly, cases were run with a Lagrangian timestep that was 50 times finer than the Eulerian timestep. Secondly, this factor was increased from 50 to 500. This proved to help with numerical stability but came at the expense of noticeable increase in computational cost. For the former case, computations completed in a timeframe on the order of 16 hours running on 20 processors. For the latter case, this time cost increase on average by a factor of roughly 2. Running cases with artificial compressibility factors of 33, 66, and 100 respectively seemed to have no effect on improving stability for the cases here attempted.

Conclusion

Completing the heuristic stability analysis allowed for some informational knowledge of general trends, however, no explicit stability guarantees or criteria can be drawn from it. The result of the 5 kHz, 10 bar ambient, 15 bar amplitude simulation after changing the parameters discussed above to achieve stability is shown in Figure (5). On the physical understanding side, we observe that with high pressure fluctuation and high void fraction the natural frequency of the bubble cloud is significantly lower than the value computed by linear theory. In sum, changing the formulation of the void fraction, refining the grid, using an adaptive timestep calculation, and decreasing the ratio of Lagrangian to Eulerian timestep all had stabilizing effects on the numerics. Changing the artificial compressibility parameter had no effect for the cases studied, although it could have a significant affect for other values which weren't explored in this study. Future work will try to extend the knowledge gained from this heuristic stability analysis and apply it to real-life scenarios in the hopes that we can accurately simulate bubble cloud dynamics in the water jackets of IC engines.

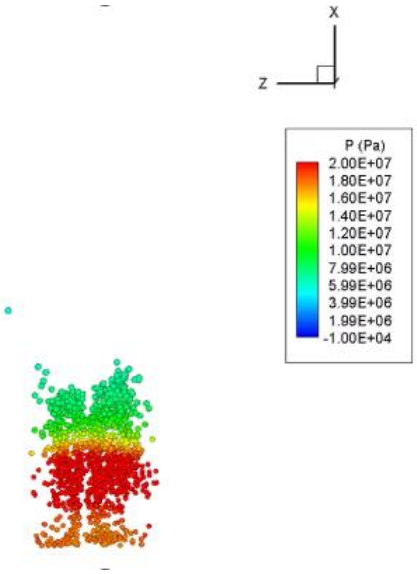

Figure (5)

References

http://www.dynaflow-inc.com/Products/Software/2_3DynaFS/Dynamics-Free-Surface-3DynaFS.htm

ANSYS Fluent Theory Guide

Brennen, C. (2013). Cavitation and Bubble Dynamics. Cambridge: Cambridge University Press. doi:10.1017/CBO9781107338760

Brennen, C., "The Amazing World of Bubbles." 8 November 2006. California Institute of Technology. The Ernest C. Watson Lecture Series. https://www.youtube.com/watch?v=FVIfAVavCpE

Ma, J., Hsiao, C. T., & Chahine, G. L. (2018). Numerical study of acoustically driven bubble cloud dynamics near a rigid wall. Ultrasonics Sonochemistry. https://doi.org/10.1016/j.ultsonch.2017.08.033.

Ma, J., Hsiao, C. T., & Chahine, G. L. (2015). Euler–Lagrange simulations of bubble cloud dynamics near a wall. Journal of Fluids Engineering, 137(4).

Plesset, M., & Chapman, R. (1971). Collapse of an initially spherical vapour cavity in the neighbourhood of a solid boundary. Journal of Fluid Mechanics, 47(2), 283-290. doi:10.1017/S0022112071001058